Spin transport in rough graphene nanoribbons

Michael Wimmer,[1,*] İnanç Adagideli,[1,*] Savaş Berber,[1,2] David Tománek,[2,1] and Klaus Richter[1]

[1] *Institut für Theoretische Physik, Universität Regensburg, D-93040, Germany*
[2] *Department of Physics and Astronomy, Michigan State University, East Lansing, Michigan 48824-2320, USA*

We investigate spin conductance in zigzag graphene nanoribbons and propose a spin injection method based only on graphene. Combining density functional theory with tight-binding transport calculations, we find that nanoribbons with asymmetrically shaped edges show a non-zero spin conductance and can be used for spin injection. Furthermore, nanoribbons with rough edges exhibit mesoscopic spin conductance fluctuations with a universal value of rms $G_s \approx 0.4e/4\pi$.

PACS numbers: 85.75.-d 73.63.-b 72.25.-b 73.22.-f

After their experimental discovery in 2004 [1], monolayers of graphite have attracted much experimental and theoretical attention owing to their unusual band structure [2]. Graphene has also been suggested as a good candidate for spin based quantum computing and spintronics [3], as it is expected to have long spin decoherence/relaxation times [4]. This prospect led to the recent interest in generating and manipulating net spin distributions in graphene, and recent experiments achieved spin injection from ferromagnetic metal contacts into graphene [5, 6, 7].

Graphene nanoribbons (GNR) are expected to show significant changes in their transport properties depending on the orientation of the edge [8]. In zigzag nanoribbons, transport properties depend typically on the existence of a state localized near the edge. Such states are visible via scanning tunneling spectroscopy [9]. Moreover, owing to their high degeneracy, these states are expected to be spin polarized [10], making zigzag GNRs attractive for spintronics [11]. Recently, transport experiments on narrow ribbons of graphene have been performed [12], however their edges were not well controlled. Recent theoretical work focused on charge transport through rough GNRs [13], but spin transport properties have not been explored yet.

In the present work, we focus on spin transport in rough zigzag GNRs. Ideal zigzag nanoribbons are not efficient spin injectors due to the symmetry between the edges with opposite magnetization. In order to achieve net spin injection, this symmetry must be broken. Existing proposals to achieve this require very large transverse electric fields [11]. We sidestep this difficulty by showing that edge imperfections (such as crystal defects or edge impurities), which usually cannot be avoided experimentally, naturally break the symmetry between the edges and lead to a finite spin conductance of the GNR. Thus, a rough zigzag GNR can be used to inject spins, or can act as a spin detector.

We start with a description of the electronic ground state properties of the zigzag GNR, which captures the essential physics relevant to spin transport. Our electronic structure results are based on *ab initio* local spin density functional (LSDA) calculations within the density functional theory (DFT), as implemented in the SIESTA code [14]. These results are mapped onto a single band tight-binding Hamiltonian [10] as

$$H = \sum_{ij,s} t_{ij} c^\dagger_{i,s} c_{j,s} + \sum_{i,s} \mathbf{m}_i \cdot c^\dagger_{i,s} \boldsymbol{\sigma}_{s,s'} c_{i,s'}, \qquad (1)$$

where $t_{ij} = t$ if i and j are nearest neighbors, $t_{ij} = t'$ if i and j are next nearest neighbors [15], and $\boldsymbol{\sigma}$ are the Pauli matrices corresponding to the spin degree of freedom. The local magnetization $\mathbf{m}_i$ can be obtained from the self consistency condition or the LSDA calculations.

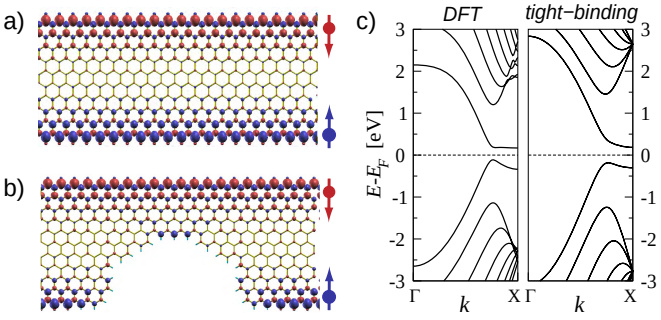

FIG. 1: (color online) Spatial profile of the ground state spin density for (a) an ideal and (b) an imperfect nanoribbon. Blue (red) corresponds to up (down) spin density. (c) Comparison between band structures of an ideal nanoribbon obtained from DFT (left panel) and tight-binding (right panel) approaches.

In the ground state, local magnetization is staggered [10, 11, 16], as shown in Fig. 1(a). At zero doping the antiferromagnetic (AF) ordering generates a gap in the single particle spectrum. We now dope the nanoribbon in order to move into a regime with open conduction channels. This can be achieved in practice by applying a gate voltage or by chemical doping. We find that a finite amount of doping reduces the AF gap and the local magnetization, but does not destroy the AF ordering. From DFT we obtain the critical value of this doping to be ≈0.5 electrons (≈0.4 holes) per zigzag edge. Furthermore, our DFT calculations showed that not only perfect zigzag ribbons, but also disordered ribbons exhibit spin polarization due to zigzag edges (Fig. 1(b)). In addition, the formation of domain boundaries at zigzag edges is

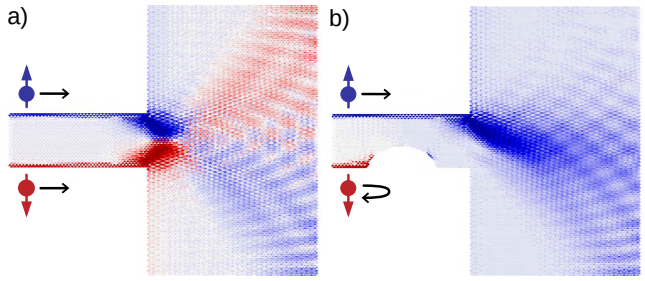

FIG. 2: (color online) Spatial spin injection profile from (a) an ideal nanoribbon and (b) a nanoribbon with a distorted edge into a region of n-doped graphene. Nonequilibrium densities of spin up (down) electrons are shown in blue (red). For an ideal nanoribbon the total spin injection vanishes, although spin Hall conductance is possible. When one of the edges has a big edge defect, the corresponding spin channel is blocked, causing nonzero net spin injection.

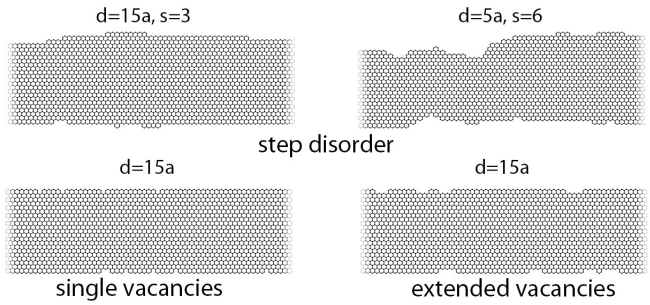

FIG. 3: Step disorder: edge disorder created by a random walk, where the width of the nanoribbon is increased or decreased by one hexagon at every step. Steps are made with probability a/d and the maximum deviation (height) from the starting point is bounded to be $\leq s$ hexagons. Single vacancies: edge disorder created by removing randomly edge atoms with probability a/d. Extended vacancies: similar to single vacancies, but also neighboring edge atoms removed. In all cases the disorder on the two edges is uncorrelated.

energetically prohibitive. In summary, our DFT calculations show that it is possible (i) to dope the GNR so that it becomes conducting and (ii) to introduce disorder at the edges while retaining the magnetic structure.

Next, we further simplify the mean field description from Eq. (1) by ignoring the variation of $\mathbf{m}_i$ within a sublattice. A spatial dependence of $\mathbf{m}_i$ changes the amount of band-bending, modifying the energy window within which the transport is predominantly through the edge states. We then obtain the single particle Hamiltonian

$$H_{mf} = \epsilon(k)\tau_1 + \Delta(k)\tau_2 + A(k)\mathrm{I} + \mathbf{m}\cdot\boldsymbol{\sigma}\tau_3, \qquad (2)$$

where $\epsilon(k)$, $\Delta(k)$ and $A(k)$ are obtained by Fourier transforming Eq. (1), and τ_i are the Pauli matrices corresponding to pseudospin(sublattice) degrees of freedom [17]. The AF exchange field $\mathbf{m}$ is obtained by fitting the band structure to that obtained from DFT (see Fig. 1(c)).

In the following, we focus on the transport properties of the GNR. We work in the linear response regime so that all the transport properties of the GNR are specified by the effective single-particle Hamiltonian (2). The spin conductance of a GNR is given by [18]

$$G_s = \frac{\hbar}{2e}(G_\uparrow - G_\downarrow) = \frac{e}{4\pi}(T_\uparrow - T_\downarrow), \qquad (3)$$

where $G_{\uparrow(\downarrow)}$ is the conductance and $T_{\uparrow(\downarrow)}$ the transmission probability for spin up (down). The conducting channels with energies closest to the undoped Fermi energy reside on a single sublattice and are fully spin polarized owing to the staggered magnetization. These states are extended along the ribbon, but localized near the (zigzag) edges of the GNR, with the spin up channel localized at one edge and the down channel on the opposite edge. The transverse localization length of these states depends on their Fermi momentum k_F that may be modified by shifting the Fermi energy E_F. As one moves away from the X point, the transverse localization length increases as $\lambda_{\mathrm{edge}} \approx -a/\ln(2\cos(k_F a/2))$, where $a = 2.46$ Å is the lattice constant of the underlying hexagonal lattice [10]. Owing to the spatial separation of the spin channels, the scattering properties of the different spins (caused e.g. by edge defects) are uncorrelated, i.e. the conductance of up spins depends solely on the impurities at the edge, where they are localized, and can be calculated independently from the conductance of the down spins. Therefore, we approximate $T_{\uparrow(\downarrow)}$ by $T_{\mathrm{l(r)}}$, where $T_{\mathrm{l(r)}}$ is the transmission probability of the left (right) edge state in a GNR, when the opposite edge has no disorder. Thus, we find that the transport properties of the zigzag nanoribbon are essentially those of two independent wires, oppositely spin polarized and connected in parallel between the reservoirs. Below, we show numerical results supporting this two-wire model in all regimes from localized to ballistic transport.

For an ideal, impurity-free GNR, we have $T_{\mathrm{l}} = T_{\mathrm{r}}$, which leads to vanishing overall spin conductance. Finite spin conductance can be obtained, however, for imperfect GNRs. As shown in Fig. 1(b), the presence of impurities does not destroy the magnetization of the edges. A single impurity will scatter the spin channel that is localized at the same edge more effectively [19], leading to a non-vanishing spin conductance. In Fig. 2 we show a quantum transport simulation using a recursive Green's function technique [21], demonstrating how one can use a GNR with a single obstacle to inject spins into bulk graphene.

From an experimental perspective, it is more realistic to consider GNRs with many impurities on both edges. In this case, the average resistance of the two spin channels is equal, quenching the ensemble-averaged spin conductance. Nevertheless, in the mesoscopic regime, sample-to-sample fluctuations in the conductance of the left and right channels will lead to a non-vanishing variance of the spin conductance.

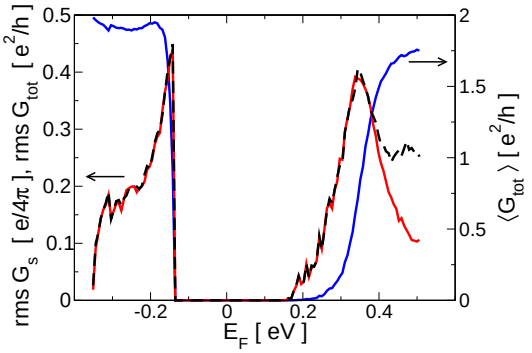

FIG. 4: (color online) Average total conductance, $\langle G_{\rm tot}\rangle$ (blue solid line), rms of the total conductance, rms G_{tot} (black dashed line), and rms of the spin conductance, rms $G_{\rm s}$ (red solid line), as a function of E_F ($E_F = 0$ is chosen to correspond to zero gate voltage). The data were averaged over 1000 configurations of single vacancies with $d = 40a$ and $L = 800a$.

Now, we use the two-wire model to relate the variances of total and spin conductance to the variance of $T_{\rm l(r)}$ as

$$\mathrm{Var}\, G_{\rm s} = \left(\frac{\hbar}{2e}\right)^2 \mathrm{Var}\, G_{\rm tot} = \left(\frac{e}{4\pi}\right)^2 (\mathrm{Var}\, T_{\rm l} + \mathrm{Var}\, T_{\rm r})\,.$$

Treating both edges as one-dimensional wires, we map the transport problem onto that of a disordered 1D chain. Transmission eigenvalue statistics in 1D disordered chains is known to be described by the Dorokhov-Mello-Pereyra-Kumar (DMPK) equation [22]. Using the full distribution function of resistance [23], we find that the universal maximum value of the root mean square (rms) spin conductance rms $G_s = \sqrt{\mathrm{Var}\, G_s} \approx 0.4e/4\pi$. In order to demonstrate this universality, we investigate GNRs of different length L and width W and various models of edge disorder (see Fig. 3). For all models, d denotes the average distance between scatterers.

First, we focus on dilute disorder, $d \gg a$. The typical behavior of the average and variance of charge and spin conductances is shown in Fig. 4. We first note that over the whole energy region, where the edge states are present, $\frac{\hbar}{2e}$ rms $G_{\rm tot} \approx$ rms $G_{\rm s}$, confirming the validity of the two-wire model. As the Fermi level is raised by gating or doping, the relevant states are extended and feel both edges. Then, the assumption of uncorrelated channels breaks down and $\frac{\hbar}{2e}$ rms $G_{\rm tot} >$ rms $G_{\rm s}$.

For an n-type GNR, when the Fermi level is near the band edge, the states at E_F are localized and both the average conductance and the fluctuations are suppressed exponentially. Raising the Fermi energy by gating or doping, we observe in Fig. 4 a crossover to the ballistic regime, where the conductance rises until the quantum limit of conductance $2e^2/h$ is reached. Correspondingly, we see a maximum in the conductance fluctuations before they vanish again in the ballistic regime.

The average/fluctuations of the conductances of a p-doped GNR are different from an n-doped one, but a description based on the DMPK equation holds well for either case. The scattering strength of impurities depends on the overlap of the impurity potential with the unperturbed channel wavefunction and therefore on $\lambda_{\rm edge} = \lambda_{\rm edge}(E_{\rm F})$. In the n-doped GNR, there is one channel whose momentum is a monotonic function of E_F. On the other hand, in the p-doped GNR, due to the band bending (Fig. 1), there are two channels: One localized near the edge, the other extended further into the ribbon, but still with a considerable density at the edge. Lowering E_F thus localizes one state even more towards the edge, whereas the other state spreads out, making the density more uniform. This leads to different functional dependences of the localization length on the Fermi energy for n- and p-doped ribbons.

In order to compare n- and p-doped ribbons as well as different disorder models, we extract the energy dependence of the longitudinal (transport) localization length $\xi(E_{\rm F})$ from $\exp(\langle ln(G_{\uparrow/\downarrow}(E_{\rm F}, L)\rangle) = \exp(-2L/\xi)$ [24, 25], as shown in the inset of Fig. 5(a). In Fig. 5(a) we show rms $G_{\rm s}$ as a function of ξ/L for all three disorder models (see Fig. 3) with different values of d and a wide range of ribbon lengths L. The data collapse on a single curve, demonstrating the universality of the spin conductance fluctuations (SCF), independent of the particular type of edge disorder. Slight deviations from this universality can be observed in Fig. 5(a), in the ballistic regime for the special case of single vacancies. In this case, the system reaches the ballistic limit only for high Fermi energy values where the two-wire model breaks down. The rms spin conductance of the n-doped GNR agrees very well with the results obtained from the DMPK equation. For the p-doped ribbon, where there are two conducting channels, we see a small increase in the rms conductance, presumably due to the crossover to a multi-channel quasi-1D wire, where rms $G \approx 0.52$ [25]. In Fig. 5(b) we concentrate on n-doped graphene for step disorder (upper panels of Fig. 3) and show again the universality of the SCF with respect to a wide range of parameters characterizing edge roughness, ribbon length and width. There is little dependence on the ribbon width W, confirming that the observed effect is entirely due to the edges.

Currently there is not much experimental control over the edges of nanoribbons. Presumably, available GNRs have dense disorder, $d \approx a$. In this limit, the observed maximum of spin conductance fluctuations decreases. The inset of Fig. 5(b) shows the maximum value of the SCF as a function of average step length d for step disorder and different parameters s and L . We observe that for $d > 5a$ the SCF are independent of the maximum height of the steps. Moreover, we find that the maximum value of the SCF is retained for $d \gtrsim 5a$. As an example, a sample disordered in the way shown in the upper right corner of Fig. 3 can show spin conductance $\approx 0.4e/4\pi$. The finite spin conductance of GNRs predicted above can be measured e.g. by attaching ferromagnetic leads in a

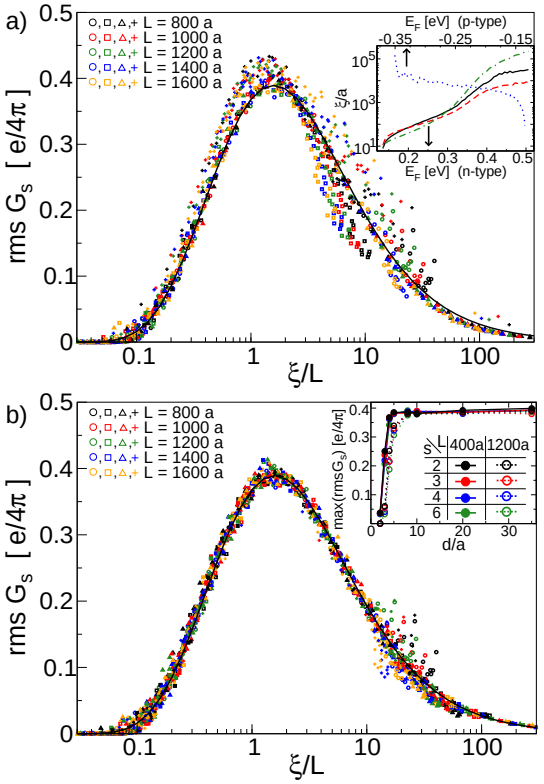

FIG. 5: (color online) Spin conductance fluctuations: (a) rms G_s as a function of ξ/L for n- and p-doped graphene: step disorder for n-type, $d = 20a$, $s = 3$ (◯), single vacancies for n- and p-type, $d = 40a$ (□ and +, respectively) and extended vacancies for n-type, $d = 30a$ (△). In the inset we give the reduced localization length ξ/a for step disorder (solid line), single vacancies (n-doped: dashed line, p-doped: dotted line) and extended vacancies (dashed-dotted line). (b) rms G_s as a function of ξ/L for step disorder in n-doped graphene: $d = 20a$ and $s = 3$ (◯), $d = 35a$ and $s = 2$ (□), $d = 35a$ and $s = 6$ (△), $d = 20a$ and $s = 6$ (+). The inset shows the maximum value of rms G_s as a function of d/a for the step disorder for different parameters s and L. In both (a) and (b), open (filled) symbols correspond to GNRs with $W = 21$ (61) hexagons and the result from the DMPK equation is represented by a solid line. The rms conductances have been estimated from 1000 ($W = 21$) and 750 ($W = 61$) disorder configurations.

two- or four-probe conductance measurements similar to Ref. [5], with one lead being a zigzag GNR, or by non-contact magnetization measurements.

In conclusion, we have discussed the magnetization of the edge states in graphene nanoribbons. We have shown that, although an ideal GNR has zero spin conductance, a GNR with imperfect edges exhibits a finite spin conductance owing to the fluctuations of the spin conductance. These fluctuations are universal with a maximum rms conductance $\approx 0.4e/4\pi$. Thus, graphene nanoribbons can be used as an efficient alternative to ferromagnetic leads towards achieving all-graphene spintronics devices.

We thank B.J. van Wees, A. Morpurgo and M. Shiraishi for discussions. I.A., M.W., S.B. and K.R. acknowledge financial support by DFG (SFB 689 and GRK 638). D.T. acknowledges financial support by NSF NIRT grant ECS-0506309, NSF NSEC grant EEC-425826, and the A. v. Humboldt Foundation.

* These authors contributed equally to this work

[1] K. S. Novoselov, A. K. Geim, S. V. Morozov, D. Jiang, Y. Zhang, S. V. Dubonos, I. V. Grigorieva, and A. A. Firsov, Science **306**, 666 (2004).

[2] A. K. Geim, and K. S. Novoselov, Nature Mat. **6**, 183 (2007); M. I. Katsnelson, Mater. Today **10**, 20 (2007); A. H. Castro Neto, F. Guinea, N. M. R. Peres, K. S. Novoselov, and A. K. Geim, arXiv:0709.1163v1

[3] B. Trauzettel, D. V. Bulaev, D. Loss, and G. Burkard, Nature Phys. **3**, 192 (2007).

[4] H. Min, J. E. Hill, N. A. Sinitsyn, B. R. Sahu, L. Kleinman, and A. H. MacDonald, Phys. Rev. B **74**, 165310 (2006); D. Huertas-Hernando, F. Guinea, and A. Brataas, Phys. Rev. B **74**, 155426 (2006)

[5] N. Tombros, C. Jozsa, M. Popinciuc, H. T. Jonkman, and B. J. van Wees, Nature **448**, 571 (2007).

[6] S. Cho, Y.-F. Chen, and M. S. Fuhrer, arXiv:0706.1597v1

[7] M. Ohishi, M. Shiraishi, R. Nouchi, T. Nozaki, T. Shinjo, and Y. Suzuki, Jpn. J. Appl. Phys. **46**, L605 (2007).

[8] K. Nakada, M. Fujita, G. Dresselhaus, and M. S. Dresselhaus, Phys. Rev. B **54**, 17954 (1996).

[9] Y. Kobayashi, K. I. Fukui, T. Enoki, and K. Kusakabe, Phys. Rev. B **73**, 125415 (2006); Y. Niimi, T. Matsui, H. Kambara, K. Tagami, M. Tsukada, and H. Fukuyama, Phys. Rev. B **73**, 085421 (2006).

[10] M. Fujita, K. Wakabayashi, K. Nakada, and K. Kusakabe, J. Phys. Soc. Jpn. **65**, 1920 (1996).

[11] Y.-W. Son, M. L. Cohen, and S. G. Louie, Nature **444**, 347 (2007).

[12] M. Y. Han, B. Özyilmaz, Y. Zhang, and P. Kim, Phys. Rev. Lett. **98**, 206805 (2007); Z. Chen, Y.-M. Lin, M. J. Rooks, and P. Avouris, arXiv:cond-mat/0701599v1.

[13] I. Martin and Y. M. Blanter, arXiv:0705.0532v2; F. Sols, F. Guinea, and A. H. Castro Neto, arXiv:0705.3805v1.

[14] P. Ordejón, E. Artacho, and J. M. Soler, Phys. Rev. B **53**, R10441 (1996); J. M. Soler, E. Artacho, J. D. Gale, A. García, J. Junquera, P. Ordejón, and D. Sánchez-Portal, J. Phys.: Condens. Matter **14** 2745 (2002)

[15] P. R. Wallace, Phys. Rev. **71**, 622 (1947); K. Sasaki, S. Murakami, and R. Saito, Appl. Phys. Lett. **88**, 113110 (2006).

[16] S. Okada and A. Oshiyama, Phys. Rev. Lett. **87**, 146803 (2001).

[17] F. D. M. Haldane, Phys. Rev. Lett. **61**, 2015 (1988).

[18] The unit of spin conductance is $e/4\pi$, in contrast to the spin-resolved charge conductance $G_{\uparrow,\downarrow}$, which is e^2/h. In this notation, the dimension of the spin current is angular momentum per unit time and that of the spin-resolved current is charge per unit time.

[19] For this, it is essential to choose $t' \neq 0$, resulting in a dispersion for the edge state. Within the energy window due to band-bending, the edge states are strongly affected by edge defects. For $t' \to 0$ this energy window reduces to the Dirac point. Therefore, numerics in nearest-neighbor

approximation away from the Dirac point can be misleading, as it suggests that the edge state is not much influenced by edge defects [20].

[20] F. Munoz-Rojas, D. Jacob, J. Fernandez-Rossier, and J. J. Palacios, Phys. Rev. B **74**, 195417 (2006); L. P. Zarbo, and B. K. Nikolic, arXiv:0704.2419v1.

[21] A. MacKinnon, Z. Phys. B **59**, 385 (1985).

[22] O. N. Dorokhov, JETP Lett. **36**, 318 (1982); P. A. Mello, P. Pereyra, and N. Kumar, Ann. Phys. (NY) **181**, 290 (1988).

[23] Eq. (20) in M. E. Gertsenshtein and V. B. Vasil'ev, Theor. Probab. Appl. **4**, 391 (1959); Eq. (4.3) in C. W. J. Beenakker and J. A. Melsen, Phys. Rev. B **50**, 2450 (1994).

[24] P. W. Anderson, D. J. Thouless, E. Abrahams, and D. S. Fisher, Phys. Rev. B **22**, 3519 (1980).

[25] C. W. J. Beenakker, Rev. Mod. Phys. **69**, 731 (1997).